

DEVELOPMENT OF A VARIABLE-SPAN MORPHING WING

Pedro Gamboa¹, Pedro Santos², Lino Miguel³

LAETA-UBI/AEROG, University of Beira Interior, Department of Aerospace Sciences
Calçada Fonte do Lameiro, 6200-358 Covilhã, Portugal

e-mail: ¹pgamboa@ubi.pt, ²p_daniel_santos@hotmail.com, ³lino.d.r.miguel@gmail.com

Key words: morphing aircraft, variable-span wing, MDO, UAV, flight testing

Abstract. *This paper describes the development and testing of a variable-span morphing wing (VSW) concept aimed at improving the performance of a small UAV which flies in the speed range 11m/s to 40m/s. An in-house aerodynamic shape optimization code, which uses a viscous two-dimensional panel method formulation coupled with a non-linear vortex lattice algorithm and a sequential quadratic programming optimization routine, is used to solve a drag minimization problem to determine the optimal values of wing span for various speeds of the vehicle's flight envelope while subject to geometric constraints. An analysis is also developed and performed to compute the roll rate available with asymmetric span control of the VSW. A full scale prototype is built for bench testing the wing/actuator system. The wing is built in composite materials and is made of two parts. An electro-mechanical actuation mechanism is developed using an aluminium rack and pinion system driven by two servomotors. Bench tests, performed to evaluate wing under load, showed that the system is capable of performing the required extension/retraction cycles and is suitable to be installed on a previously developed UAV airframe which has been modified and instrumented to serve as the test bed for evaluating the VSW concept prototype in-flight.*

1 INTRODUCTION

The development of morphing wing technologies for flight regime adaptation has received great interest from researchers and engineers in the past years. The design of adaptive mechanisms and structures, along with the development of smart materials that allow bio-mimetic configurations of aircraft is highly desired in the near future. The new concepts and technologies developed up to now are a constant attempt to enhance the overall flight performance of aircraft, enabling new aircraft design approaches to be pursued and opening grounds for improved multi-mission flexibility. This enhancement in performance capability was clearly demonstrated by Tidwell *et al* [1].

Most morphing concepts perform changes in aircraft shape during flight and comprise the structure and the systems which perform those changes. Methods for airfoil and wing morphing include camber change [2], variable-twist, wing sweep change, and wing span change [2,3], for example. Several different concepts have been designed and tested in this field: from the pneumatic telescopic spars by Blondeau *et al* [4] and the inflatable wings by Cadogan *et al* [5] and Scarborough *et al* [6], to the telescopic wing servo/pulley-actuated by Vale *et al* [7], among many others. Flight testing of a telescopic wing in a manned sailplane was conducted by the Akademische Fliegergruppe Stuttgart*. A different concept, a batwing morphing concept from NextGen, has also been validated in flight after extensive design and wind tunnel testing [8,9]. Henry *et al* explored as well the effects on UAV stability caused by asymmetric span variations [10]. Since such a wing is very structurally demanding, Bae *et al* [11] proposed an aeroelastic and aerodynamic analysis of a variable wingspan for a cruise missile. Neal *et al* went further and built a fully adaptive model with seven degrees of freedom [3]. Many projects have been done on aircraft morphing concepts, and much work is being carried out in this field: enhanced performance and increased energy efficiency of aircraft is of extreme importance and drive the research [12].

Overall system performance of such concepts is not easily grasped and therefore optimization techniques are required during the design process. During concept development, even iteration between design and experiment is important. Much work has been done on aerodynamic shape optimization of airfoils and wings and multidisciplinary design optimization of wing systems [2,13,14] in order to enable shape changes to improve flight performance.

The development of unmanned air vehicles (UAVs) and its recent increasing applications in many areas, both military and civil, is a result of their huge potential to perform distinct missions without direct risk to the crew, of their great deploying capability and also of their lower development and production costs relative to manned aircraft. The use of such vehicles to develop and test new concepts for performance enhancement is, therefore, very attractive.

This paper describes the work done in the design, development and testing of a variable-span morphing wing concept aimed at improving the flight performance of a small UAV relative to the performance obtained with a conventional fixed wing.

2 DESIGN AND OPTIMIZATION

The main goal of this work is to design a wing for a small UAV that can perform in-flight span variations, a variable-span wing (VSW), in order to reduce wing drag at a given flight speed. The aircraft fitted with the VSW should be capable of operating in

* From the web site <http://www.uni-stuttgart.de/akaflieg/en/projects/all-fs-projects/fs-29-tf.html>, March 2012.

the same range of speeds as with the original wing, from about the stall speed of 11m/s to 40m/s, with similar performance at low speed but better performance at high speed. Asymmetric span deployment should be sufficient for roll control. The UAV under study is an experimental UAV developed by the Aerospace Sciences Department of University of Beira Interior. It is a high-wing pusher aircraft, with an electric brushless motor configured for 420W, and the propeller placed behind its V-tail. The original wing structure is made of balsa wood ribs, a balsa wood torsion box and hard wood spars. The takeoff weight of the aircraft, W , is 60N. The original rectangular wing has a constant chord, c , of 0.25m and a planform area, S , of 0.625m². The airfoil used is a SG6042, a low speed airfoil with a good compromise between maximum lift coefficient and design simplicity. The cruise speed of the aircraft is about 20m/s, and maximum speed about 40m/s.

The shape and size of the VSW was obtained through a computational constrained aerodynamic shape optimization aimed at determining the wing chord and span values that minimized its drag for a given speed range. The geometric constraints imposed on the wing design optimization were dictated by component fitting, manufacturing simplicity and mechanism functionality considerations. A brief description of the optimization procedure and of the main results is given below but more detailed information can be sought in [15].

2.1 Aerodynamic Analysis and Optimization

Simple medium-fidelity aerodynamic analysis algorithms were implemented and integrated with other shareware aerodynamic analysis programs and optimization algorithms in order to assemble the wing aerodynamic shape optimization tool.

The aerodynamic analysis implemented in the code is done in two steps. First, the 2-dimensional (2D) aerodynamic coefficients as functions of angle of attack (AOA) and Reynolds number (Re) at specified wing sections across the span of the wing are obtained using the solver of the XFOIL code [16]. Then, a non-linear lifting-line method [15,17,18] or a non-linear vortex lattice method (VLM) is used to obtain the lift distribution and the induced drag. The VLM algorithm implemented is based on the steady linear VLM [19] and is coupled with an iterative decambering approach [20]. In calculating the total lift of the vehicle it was assumed that only wing and horizontal tail contribute to lift. The tailplane lift is calculated such that the pitching moment about the centre of gravity (assumed at wing quarter chord position) is zero. Therefore, for a negative wing pitching moment, typical of positive cambered airfoils, the wing lift must be greater than the weight to compensate for the negative tail lift. This affects not only the induced drag of the wing but also the parasite drag since it flies at a higher AOA.

In this tool, empirical weight information for the wing, the tailplane and the vertical tail was introduced to allow for the variations in airfoil relative thickness, wing area, aspect ratio and taper ratio. The weight formulation is based in [21] and is described in [15].

The gradients of the objective function and constraints are a requirement of any gradient-based optimization algorithm. In this work, the gradients are computed using forward finite-differences, which enables the problem of finding the gradients to be treated as a black box. Therefore it can be used with any fluid flow solver because it does not involve changes in the solver's code.

The constrained aerodynamic shape optimization is carried out with the sequential quadratic programming (SQP) constrained optimization algorithm of FFSQP3.7 [22]. SQP has been shown to produce good results [23].

2.2 Aerodynamic Shape Optimization

The variable-span wing planform geometry is illustrated in Fig. 1. In this study, the wing does not exhibit any dihedral or any sweep (the quarter chord line lies along the y -axis) and is made of one rectangular inboard part (inboard fixed wing – IFW) and a rectangular outboard part (outboard moving wing – OMW) which slides in and out of the IFW for span changes. Taking into account fuselage dimensions and the geometric characteristics of the wing, four wing sections were defined from the root to the tip for the optimization problem, as shown in Fig. 1, where the lateral position of station 4 is the only one allowed to vary during the optimization process. The positions of sections 2 and 3 are automatically defined given the highest value of the position of section 4 (maximum semi-span) in such a way that the OMW when fully retracted fits completely inside the IFW (between fuselage side and section 3) and when fully extended maintains a 0.1m overlap with the IFW for structural reasons. The maximum wing span is 2.5m, the same value as in the original fixed wing.

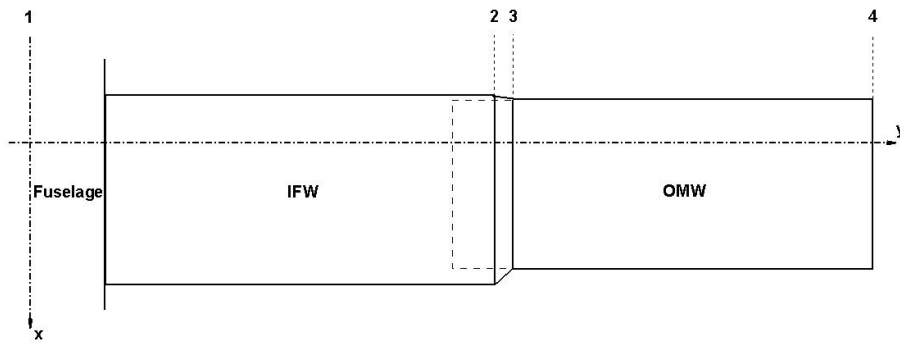


Figure 1: Variable-span wing planform.

Several optimization problems were studied [15] but, for brevity, only the one that led to the implementation of the wing prototype is presented here. In this case the OMW airfoil is a SG6042 airfoil modified to have a straight lower surface, the OMW chord length is fixed and equal to 0.25m and no stall speed constraint is imposed. The optimization statement is shown below, for two sets of design variables, span and AOA, where the angles are in degrees.

Minimize:
$$f = \int_{V_i}^{V_f} D(\alpha, b, V) dV \quad (1)$$

Subject to:
$$\begin{aligned} L(\alpha, b, V) &= W \\ -5 &\leq \alpha \leq 20 \\ 1.475 &\leq b \leq 2.5 \end{aligned} \quad (2)$$

In the objective function of Eq. (1), the integral between the initial and final speed values, V_i and V_f , respectively, was calculated using Simpson's Rule where D was computed at five speeds: 15m/s, 20m/s, 25m/s, 30m/s, and 35m/s. For each one of these speed values there are two design variables, AOA and span, totalling 10 design variables for this optimization problem. For the wing fully extended the increase in wing weight was computed as 3.6N resulting in a takeoff aircraft weight of 63.6N. For the OMW fixed chord of 0.25m the IFW chord resulted in 0.2822m. Based on the aerodynamic shape optimization results, the plots of Fig. 2 were obtained for the VSW

and the original fixed wing.

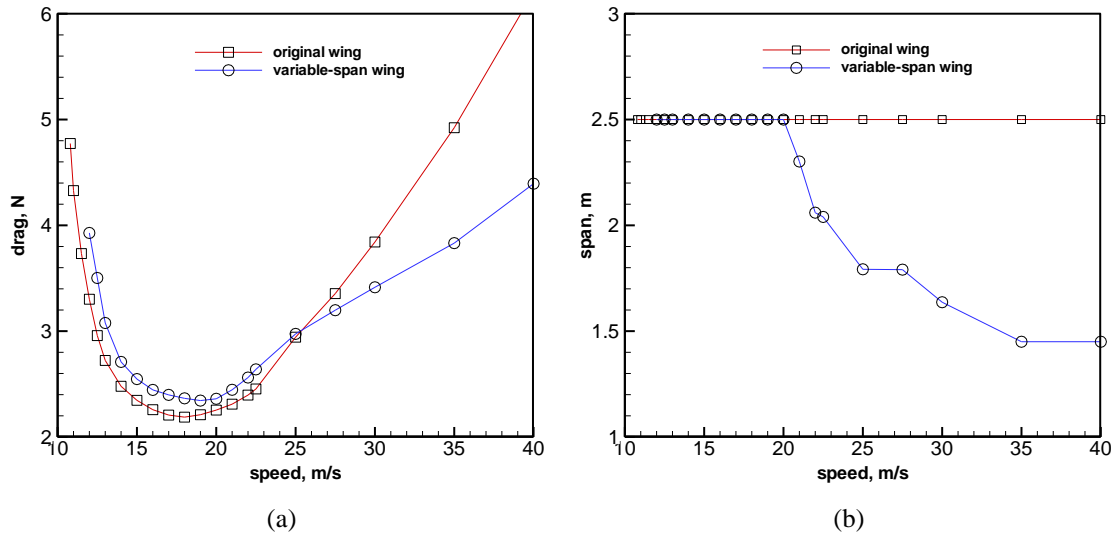


Figure 2: Numerical comparison between original and variable-span wings (results obtained with the non-linear VLM code): (a) wing drag, and (b) span variation with speed.

In Fig. 2(a) one can see that the VSW has better performance than the original wing only at speeds above 25.5m/s, indicating that the present design allows better performance at the higher speed end of the envelope. At 30m/s the VSW has about 10% less drag than the original one. At a speed of 40m/s the drag reduction increases drastically to 28%. At low speeds, the original wing outperforms the new wing, although presenting only slightly better results. The original wing was designed for low speeds, and near the design point it was expected to have better performance than the new wing because of the higher relative thickness of the airfoil in the IFW and because of the less efficient airfoil used. Therefore, the new wing presents a slightly higher total drag at low speeds when it is fully extended, which is only compensated at higher speeds, when the wingspan starts to decrease. For example, one can see that above 20m/s a major span reduction takes place (see Fig. 2(b)), when the new wing performance surpasses the original wing, until the minimum span of 1.475m is reached at a speed of 35m/s. Stall speed increased too, from 10.75m/s in original wing to 11.5m/s in the new wing. The increased weight of the wing had an important effect in the wing performance at low speeds.

Fuselage drag was not considered in this study but clearly the smaller variation in AOA of the VSW can result in reduced fuselage pressure drag allowing further benefits in the aircraft overall drag curve. In the range 17.5m/s to 30m/s the variation in AOA of the VSW is only around 2deg whilst that of the original wing is 4.5deg.

2.3 Roll Rate Analysis

Stability and control on morphing aircraft is always a matter of paramount importance. The changes in aircraft motion due to physical modification of the structure and also the implication that in-flight large scale changes produce on stability must be taken into account. In the case of the variable-span wing, the ability to perform large variations in span rules out the possibility to have high performance roll control through conventional ailerons. However, recent research [10,24] demonstrated that roll control by asymmetric span variation is possible.

Morphing wings in general suffer from variations in lift distribution that are not present in ordinary fixed wings. In asymmetric span changes, assuming elliptic wing lift

distribution, the centre of the ellipse moves along with the wing. Therefore, the lift distribution symmetry point moves in the direction of the larger semi-span extension. A methodology was derived to estimate the control and damping rolling moment coefficients due to asymmetric span actuation. The method is explained in detail in [15].

Applying the mathematical model derived, the plot of Fig. 3 was calculated. It can be observed that the roll rate for the variable-span wing decreases with the increase in speed, contrary to what happens in a wing with ailerons. The new wing matches the aileron performance in terms of roll power, being the maximum roll rate values similar to both wings. Figure 3 also shows that there is always a combination of asymmetric span deployment that enables the UAV to overcome a minimum roll rate value of 46.15deg/s [25]. One can conclude that roll control is possible with asymmetric span variations and that the variable-span wing is capable of performing steady turns. One problem that may arise in a practical implementation of the VSW is the time response of span variation, which for reasonably small actuators, may increase due to higher travel and inertia of the OMW relative to conventional ailerons.

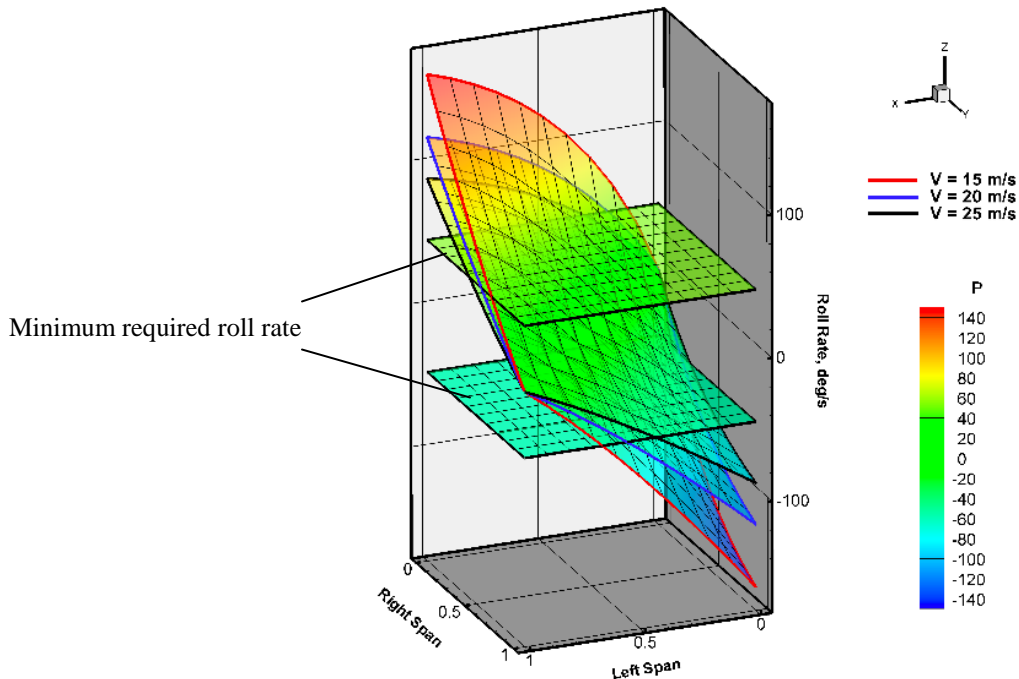


Figure 3: Roll rate behaviour at 15m/s, 20m/s and 25m/s for the variable-span wing – the two horizontal planes refer to the minimum acceptable roll rate value: 46.15deg/s.

Some analyses have been performed on simulating the response of the UAV under study fitted with the designed VSW in two different situations: one in which it was required to establish equilibrium after an initial perturbation in the state variables and another in which it was required to follow a target bank angle by controlled dissymmetric span actuation and elevator deflection [26]. Two control methods were implemented (LQR and Batz-Kleinman) both demonstrating good performance in controlling the aircraft with the required handling quality level.

3 PROTOTYPE DEVELOPMENT

Given the promising results obtained in the design optimization process a working prototype was implemented to allow the pursuit of several ground and flight validation and assessment tests. The actuation mechanism, wing structure and manufacturing

techniques used to build the structure are briefly presented below. A more detailed description can be found in [27].

3.1 Actuation Concept

The variable-span wing concept in the present work presents a very simple layout: a hollow wing (IFW) inside of which a smaller conventional wing slides (OMW) actuated by a simple electromechanical mechanism consisting of a servomotor, a pinion and rack. The pinion is driven by the servomotor installed at the centre of the wing assembly and pushes/pulls the rack which is attached to the OMW to make it slide inside the IFW. The maximum span length was set equal to the original fixed wing: 2.5m. For this total span, it was estimated that both inboard and outboard wing parts would have a length of 0.625m, and based on the experience acquired in UAV construction, that 0.1m of minimum wing overlapping would allow sufficient wing stiffness in the full extended configuration. Knowing these dimensions and fuselage width one was able to estimate the IFW and OMW lengths. The overall system was developed in a CAD/CAM tool and is illustrated in Fig. 4 where the main components are highlighted.

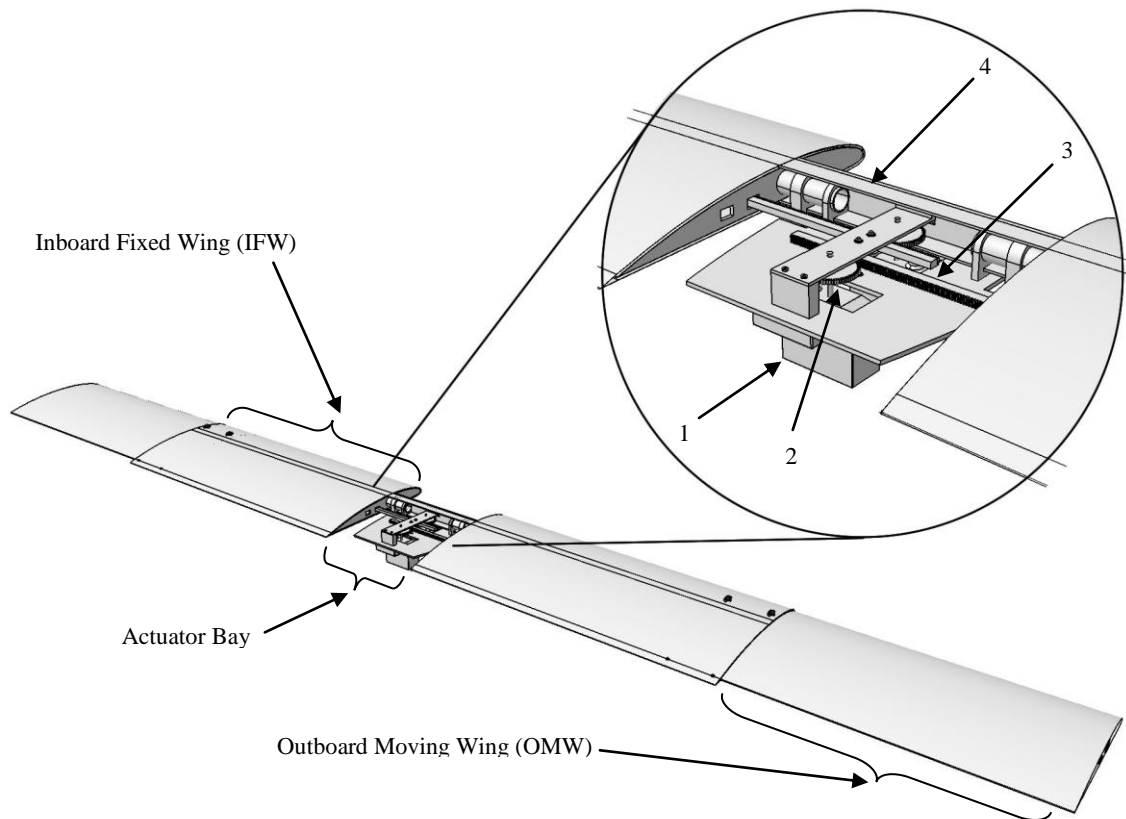


Figure 4: General CAD view of the Variable-Span Wing (VSW) showing its main components and a detail of the actuator bay: (1) servo-motor; (2) transmission pinion; (3) transmission rack; and (4) pultruded unidirectional carbon spar.

3.2 Wing Structure

The structural components of the wing were developed with a combination of composite materials and hard and soft wood which provide good general strength and stiffness. The sizing of the structure was performed with simple analytical text book formulas considering limit material stresses and required structural stiffness. An aeroelastic computational model is currently being developed to determine the critical

flutter speed.

The IFW uses a monocoque type of structure with a sandwich of carbon/foam/carbon skin which is required to both provide the correct shape and resist shear loads. From inside out, the load carrying thick skin has a layer of 48g/m² glass/epoxy, a layer of 185g/m² carbon/epoxy, a layer of 2mm porous PVC foam (55kg/m³), a layer of 185g/m² carbon/epoxy, and finally another layer of 48g/m² glass/epoxy. The PVC foam core was incorporated between the carbon fibre layers to allow embedding of the main spar and to give adequate stiffness to the skin. All fibre fabric layers are plain weave (carbon fibre with 50% warp 1K HS and 50% weft 1K HS and E glass fibre with 56% warp EC5 11 and 44% weft EC5 11) oriented at 0deg along the wing span. The glass layers are added to reduce the porosity of the carbon/epoxy layers and to allow surface sanding after curing to improve its finishing without damaging the structural carbon/epoxy layer. The complete assembled skin has a thickness of 2.5mm, which originates a fairly acceptable small discontinuity between IFW and OMW. Two Spar caps inside the IFW are composed of rectangular beams made of pultruded carbon fibre with a cross-section of 8mm×1.8mm. For greater strength and stiffness the spar spans the complete fixed wing span of 1.475m. This can be observed in Fig. 4.

The total length of the OMW is 625mm, where 525mm is the stroke and 100mm is the overlap with the IFW that remains so that bending and torsion moments can be effectively transmitted from the OMW to the IFW. The structural configuration used in the moving wing part is very conventional: the wing is composed of ten 2mm thick balsawood ribs, a 240g/m² carbon fibre/epoxy skin and a spar consisting of a pultruded carbon circular tube with an outside diameter of 22mm and a wall thickness of 1mm. The main circular spar confers sufficient bending stiffness while the ribs provide the correct wing shape. The carbon tube combines the best compromise between availability, price and specific strength. The ribs are perforated in order to attach both the circular spar and a rack-guide tube. To prevent the transmission rack from getting stuck when crossing the opposite wing ribs, this rack-guide tube is made from epoxy impregnated carbon fibre. This carbon fibre tube is bonded to the ribs in the same way as the circular spar.

3.3 Wing Prototype Construction

The hand-layup and vacuum bagging lamination approach was chosen, since this technique allows a lightweight structure to be obtained with low cost and reduced complexity. The cure process was performed under controlled temperature conditions in two steps (cure and post-cure) so that the mechanical properties of the composite parts could be known with confidence. Moulds were produced to build the various skin parts.

The VSW actuation mechanism was designed to allow in-flight extensions and retractions of the wing. A simple rack and pinion system actuated by a servomotor was selected as the best suited for the purpose: it is light and fast enough if actuated properly. In future work, development of an automatic span extension controller should be facilitated by this choice. It was the control simplicity that led to the choice of a servo-mechanism as a means to actuate the wing more than its known affordability and reliability.

The rack rod used to push/pull the OMW is made of aluminium and has a 5mm x 9mm cross-section. It is 0.8m long, which is enough to span the wing length of 0.625m and the stroke needed of 0.525m. The two elements can be observed from Fig. 5(a). In order to select the material and size of the rack several factors were addressed: weight, availability, size and price. Combining availability and weight, the material selected for

the rack was aluminium. Given that the rack is a critical element of the control system, with the fact that it is part of a moving system subject to vibrations, adding to buckling and flexural stiffness considerations and manufacturing issues, a section of 9mm x 5mm was adopted. The material selected for the pinion was bronze to reduce friction. In the future, light weight materials may be considered.

The selection of the servomotors followed again a series of considerations regarding availability, low price, high speed, high torque, low weight and incorporation of metal gears, being the latter a prerequisite to carry out the necessary modifications. Combining the best compromise, a pair of *Hitec HS-805MG* servos was purchased. The actuation shaft and the position feedback potentiometer gearing of the servo were modified to allow the right combination of speed and turns for the required motion of the OMW. Using 2nd gear stage of the servo for actuation allowed an ideal complete deployment of 1.5 seconds with a 51.97N force on the rack. The actuation pinion was fixed to the 2nd stage of the servo through a steel shaft that fitted perfectly in the spur gear recess of the 2nd stage. A new gear relation was also implemented to adjust the travel of the wing. After the modifications a speed and torque of 1111deg/s and 0.93Nm, respectively, were obtained in the 2nd gear stage. The modified servo is shown in Fig. 5(b), clearly showing the actuation pinion and the feedback potentiometer reduction gear box.

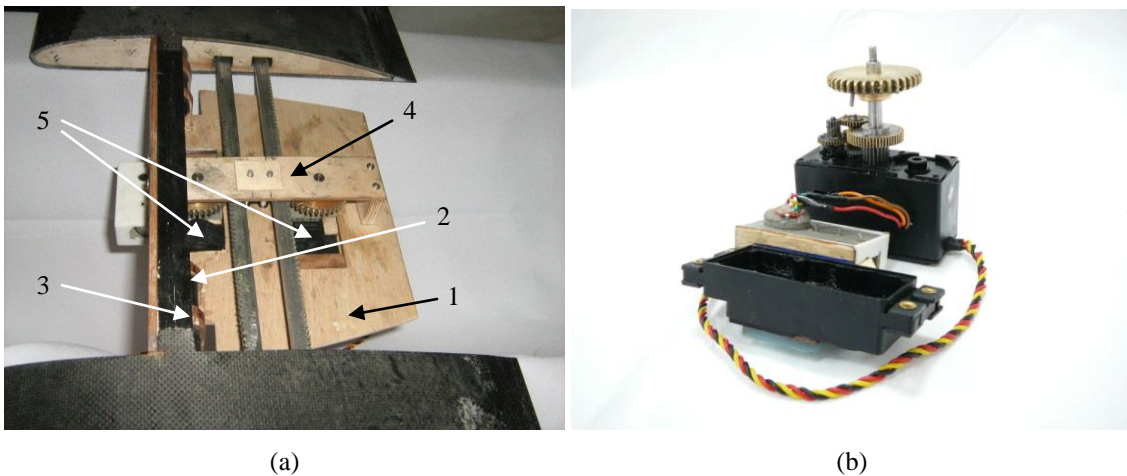


Figure 5: (a) Wing prototype: (1) servomotors supporting board; (2) board linkage; (3) wing-fuselage lug; (4) upper board and actuation bay; and (5) servomotors; and (b) Modified *Hitec HS-805MG* servo.

After the actuation system was developed, a platform capable of supporting the servos and effectively transmitting the forces to the VSW moving parts, subject to geometric constraints dictated by the fuselage size of the UAV, was built. Considering all this, the result was a plywood board 3mm thick, supported by two 6mm thick lugs of the same material bonded to the wing tube and spars as seen in Fig. 5(a). In this figure, the upper board (4) supports the pinion's shafts and the rack's guiding rollers at the top. The function of the rollers is to align and maintain the racks in contact with the corresponding pinions' teeth. In order to reduce friction to an acceptable minimum, ball bearings were placed in all contact holes between shafts and supporting structure. In order to keep the weight low, the rollers were lathe machined from a 10mm aluminium circular rod.

3.4 Wing Mass

All components were weighed in order to evaluate the difference in mass between the conventional wing and the telescopic wing. Table 1 presents the main component

masses and the total mass of the prototype wing. The resin used to impregnate the composite skins is included in the mass of the different assemblies. The wing's total mass, including the actuation mechanism, is around 1.85kg, as opposed to 1.3kg of the original wings developed for the Olharapo UAV (with the original flight control system of servos and cables and the wing supporting part that attaches to the fuselage). This is an increase of about 0.55kg: 42% of wing mass or 9% of total vehicle mass. This value represents 0.18kg more than the 0.37kg first estimated with a preliminary wing prototype and assumed in the aerodynamic optimization of the wing [15]. The increased mass was due mainly to the servos selected which had to be more powerful and hence larger than initially anticipated and to the heavier rack and pinion transmission. In the future, this negative mass margin should be reduced through structure and actuating system optimization and by improving construction techniques. For example, the transmission elements could be manufactured from a plastic or similar material.

Assembly	Mass, kg
OMW (including rack)	0.471
IFW	0.852
Actuation bay	0.459
VSW	1.846
Original Olharapo's wing	1.295

Table 1: Mass of major assemblies of the telescopic wing and mass of the original Olharapo UAV wing.

4 GROUND TESTING

Bench tests were performed to evaluate the performance of the overall system. In order to achieve this, two separate types of tests were conducted: structural and actuator system testing.

4.1 Structural Tests

Structural tests were performed with the objective of evaluating the strength and stiffness of the VSW. More specifically, the wing tip deflection was measured when subjected to different loads representing a range of flight load factors. The flight loads were simulated by placing sand bags on the lower surface of the wing with t placed upside down on a stand. For simplicity, the wing load distribution was considered constant in the IFW and triangular in the OMW portion. Load factors between 0G and 4.5G were applied. Furthermore, all the sand bags were distributed along the main wing spar in order to avoid unnecessary torsion of the telescopic wing assembly. The tip deflection was determined by reading off a scale placed behind the wing tip. Figure 6 shows the assembly used to carry out the tests and the loads applied to represent two different load factors.

The increase in load factor led to a considerable increase in the wing tip vertical deflection. Also, a slight slope discontinuity was observed at the position where the movable wing enters the fixed wing, particularly at higher load factors. However, the OMW showed to be quite stiff. The overlap of 100mm between both wing parts resisted the bending loads by deforming the airfoil contour shape: effectively increasing the airfoil thickness. This localized bending produced a small gap between the IFW upper skin and the OMW upper skin which became more apparent at higher load factors, reaching a value close to 2mm under a 4.5G load. This situation needs to be solved by increasing local stiffness (either by placing an outer rib or by substituting a strip of the foam core with a carbon/epoxy strip with the same thickness at the IFW tip and 0.1mm inboard where the bending moment from the OMW is reacted by the IFW at full span)

to avoid undesirable flow induced vibrations.



Figure 6: Variable-span wing loaded at: (a) 3.5G – 10.5kgf; and (b) 4.5G – 13.5kgf.

The variation in tip deflection with increasing load factor is shown in Table 2. It should be noted that for load factors of 3.5G and 4.5G, the tip deflection was about 39mm and 55mm, respectively, showing an overall good stiffness to bending. The deflections reached these values, in part, due to the lack of skin stiffness at the interface of the OMW with the IFW.

Load Factor	0	1	2	3.5	4.5
Tip Deflection, mm	0	6	18	39	55

Table 2: Wing tip vertical deflection as a function of load factor.

4.2 Actuation System Tests

Two types of tests were performed to the actuation system to measure the time of actuation and the energy efficiency of actuation.

The objective of the actuation force test was to measure the maximum force that the actuation mechanism could hold. In order to achieve this, the assembly shown in Fig. 7 was used. The rack was installed in the actuator, without the OMW, a string was attached to its tip and supported by a roller that converts the horizontal motion into a vertical one. At the end of the vertical part of the string, weights with successively increasing value, were hung until the system actuator was no longer able to raise them. Following that procedure, it was determined that the maximum weight lifted by the servo mechanism was 39.2N. The servo torque corresponding to this weight is 0.71Nm, which is below the expected 0.93Nm as indicated by the servo manufacturer. This represents a value 24% lower than expected. Two distinct factors contributed to this result: the high current drain imposed by the servomotor led to a drop in the supplied voltage and also the existence of imperfections of the rack-pinion assembly, mainly imperfections in the rack teeth. The latter contributed to significant energy being lost that could otherwise be used to move the wing.

The actuation time test aimed at measuring the telescopic wing extension and retraction times for various load factors. The approach used during the structural bending tests, where weights were placed over the OMW, was not appropriate in this case, because this part of the wing was required to slide inside the IFW during the actuation sequence. For this reason, instead of loading the OMW with the triangular

load distribution an equivalent concentrated force was placed at the wing tip. The equivalent concentrated force was calculated so that its moment at the OMW/IFW interface was the same as that of the normal load distribution.

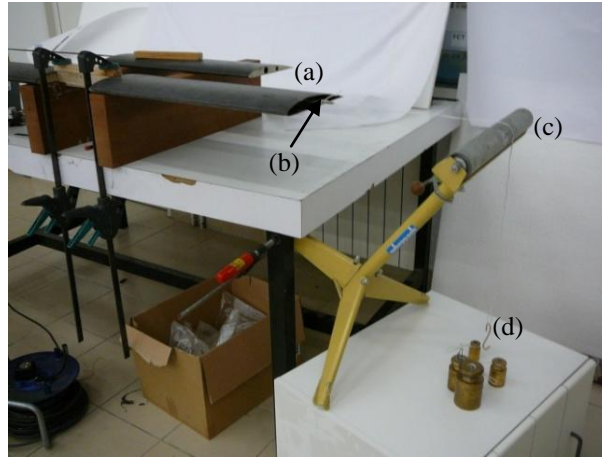


Figure 7: Installation used to measure the maximum force that the actuation mechanism could hold. It is possible to observe the different equipment employed during the test: (a) VSW without OMW; (b) rack; (c) roller support; and (d) loading weights.

Full cycle times (extension followed by retraction) were measured using a digital stopwatch. The results of half-cycle actuation times for different load factors are shown in Table 3. It becomes clear that the time of retraction/extension increased as load factor was raised. This was already expected, since increasing the load factor increases friction between wing parts and hence the servomotor had more difficulty in overcoming the increased force.

Load Factor	0	1	2	3	4
Time, s	1.8	2.0	2.3	2.5	3.0

Table 3: Half-cycle actuation times for *Hitec* HS-805MG servos.

To determine the mechanism efficiency, two separate measurements for various load factors, ranging from 0G to 4G, were performed. These tests were: (a) evaluating the energy consumed by the system, and (b) evaluating its useful work.

In order to carry out the first test (a), an *e-logger V3* from *Eagle Tree Systems*TM was used to determine the power consumed by the servomotor. This device measured the maximum, minimum and average values of current and voltage levels, over the prescribed period of time, with a refresh rate of ten readings per second. In order to ensure a point of comparison between the various load factors, a radio emitter *Multiplex Royal EVO 9* in *test run* mode was used, being the selected period time about 30 seconds. When selected in the *test run* mode, the RC transmitter sends a signal such that the servo oscillates between the determined position values corresponding to the desired time. System current and voltage were obtained for various load factors (Fig. 8). Using the measured current and voltage, the power consumed by the servomotor was determined (Table 4).

In the second test, the average actuation force and total deployment time was measured, in order to obtain the useful work. The methodology of this test needed to guarantee that both tests, (a) and (b), were comparable. The procedure selected made use of a load cell and registered its voltage output level over time. One of the two servos of the wing was used to pull the load cell connected, on the other end, to the OMW. For

a stable motion, the cell was mounted along a guide aligned with the VSW, ensuring a correct measurement of the force. The load cell signal was registered by a *Picoscope2000* from *Pico Technology*TM and later converted into force through a program written in FORTRAN. From the force variation measured over the test interval its average was calculated. The assembly for this test is shown in Fig. 9. After carrying out the tests of servomotor consumption and system useful work, it was possible to determine the VSW system efficiency.

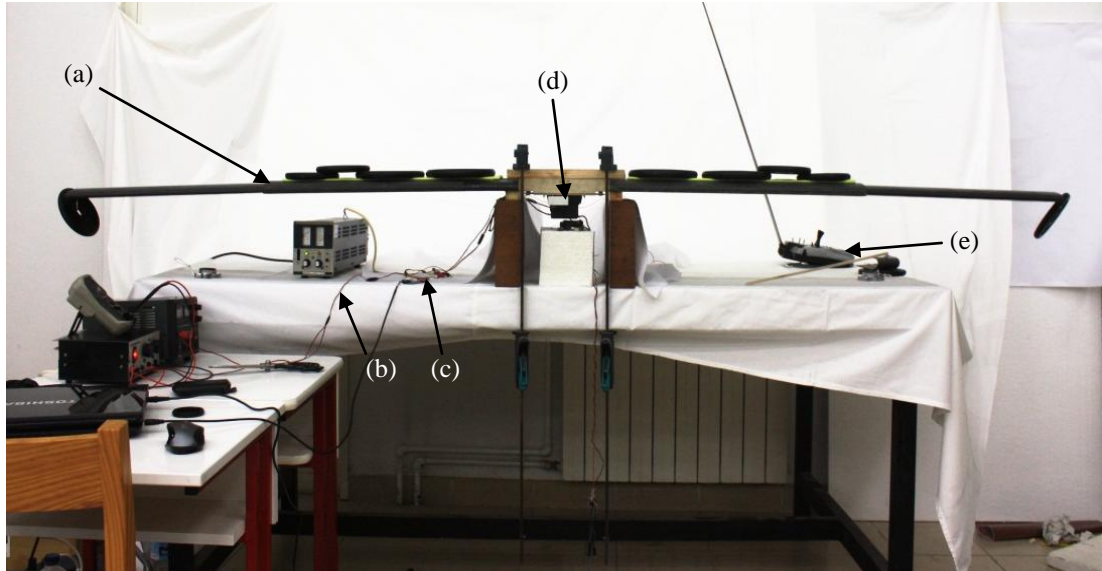


Figure 8: Test assembly used during power consumption determination. It is possible to observe the different equipment employed during the test: (a) VSW; (b) power source; (c) *e-logger V3*; (d) servomotor assembly; and (e) RC transmitter.

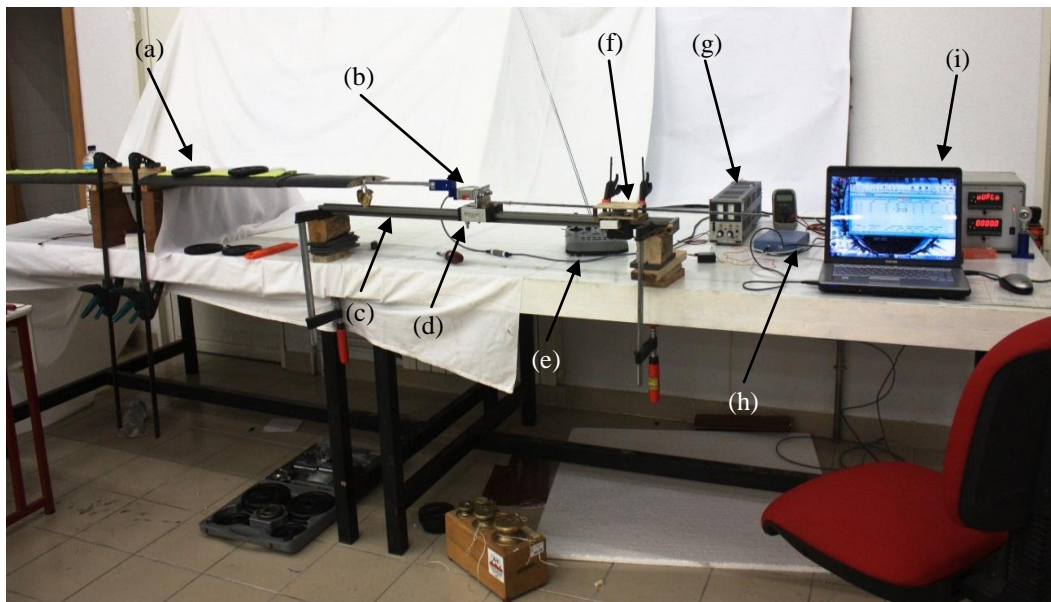


Figure 9: Test assembly used in the mean force determination. It is possible to observe the different equipment utilized during the test: (a) VSW; (b) load cell; (c) plus; (d) linear bearings; (e) RC transmitter; (f) servomotor assembly; (g) power source; (h) *Picoscope2000*; and (i) portable computer with *Pico Technology*TM recording software.

A summary of the test results for various load factors can be found in Table 4. We can observe the expected increase in power consumption due to the higher wing loading

and the consequent friction increase. On the other hand, as load factor increases the efficiency decreases. The explanation for that lies in the servomotor, since the high current drain, imposed by the high torque output, reduces its efficiency. The major energy loss is due to heat. In fact during the high load factor tests, a cooling system had to be setup in order to avoid servomotor over heating. One other factor that could also contribute to this efficiency reduction, are small construction imperfections that were more apparent when the VSW worked under higher load factors.

Load Factor	Power, W	Time, s	Servo Energy, J	Useful Servo Work, J	Efficiency, %	Average Voltage, V	Average Force, N
0	2.34	30	70.3	31.7	45	5.75	4.81
1	3.76	30	112.9	40.5	36	5.81	6.62
2	5.79	30	173.6	57.6	33	5.76	9.73
3	7.60	30	228.0	68.6	30	5.73	13.27
4	9.49	28	265.8	73.7	28	5.71	17.25

Table 4: Consumption and efficiency test results.

5 FLIGHT TESTING

Flight tests are currently being prepared to evaluate in-flight system functionality, roll control authority, energy requirements for actuation during a typical mission profile, and relative performance of the UAV fitted with either the VSW or the original conventional wing.

5.1 UAV Test Bed

A UAV airframe developed in previous works was adapted to receive the VSW and to be fitted with the necessary systems to measure in-flight parameters and communicate them back in real time to a ground control station.

The tail of the UAV was redesigned from its original V-tail configuration to an equivalent H-tail configuration to allow the UAV to perform safe roll manoeuvres with rudder and elevon deflections (asymmetrical deflection of elevator) without the need for aileron actuation. The VSW, which does not possess ailerons for structural simplicity and improved aerodynamic performance, produces rolling moments by asymmetrical wing deployment. The tail modification was implemented to allow for extra roll power during initial performance tests with wing symmetrical only deployments and should the speed of wing actuation be insufficient to adequately control the vehicle in roll. The UAV fitted with the original fixed wing and with the telescopic wing placed at three different span positions is shown in Fig. 10.

A large number of parameters are required to characterize the flight status of the vehicle and its propulsion system in order to assess the performance of the wing. The main parameters of interest are: airspeed; air density; altitude; angles of attack and sideslip; pitch, roll and yaw angles; motor speed, voltage and current; propeller thrust; and VSW servos voltage and current, among others. To collect all these data an *ArduPilot Mega 1.0 (APM1.0)* is used. This platform is used given its versatility and completeness. In fact, it has an inertial measuring unit, barometric and temperature sensors, airspeed sensor and also a wireless data link capable of bidirectional data communication with the ground control station (*QGroundControl*). The ground station software allows real-time monitoring and visualization and also enables the data to be saved for ulterior analysis.

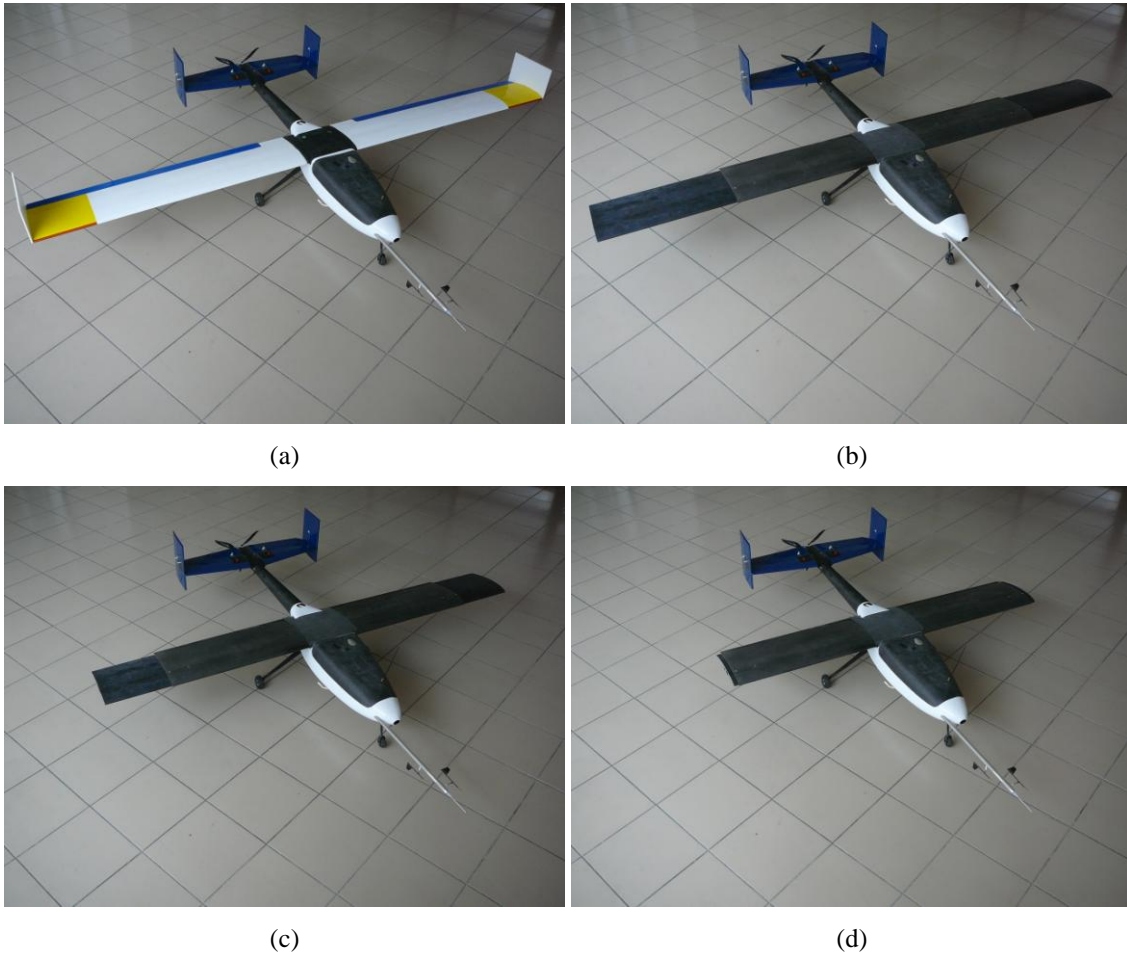


Figure 10: UAV platform fully instrumented for performance assessment of the VSW: (a) original fixed conventional wing; (b) VSW wing fully extended; (c) VSW in intermediate position; and (d) VSW fully retracted.

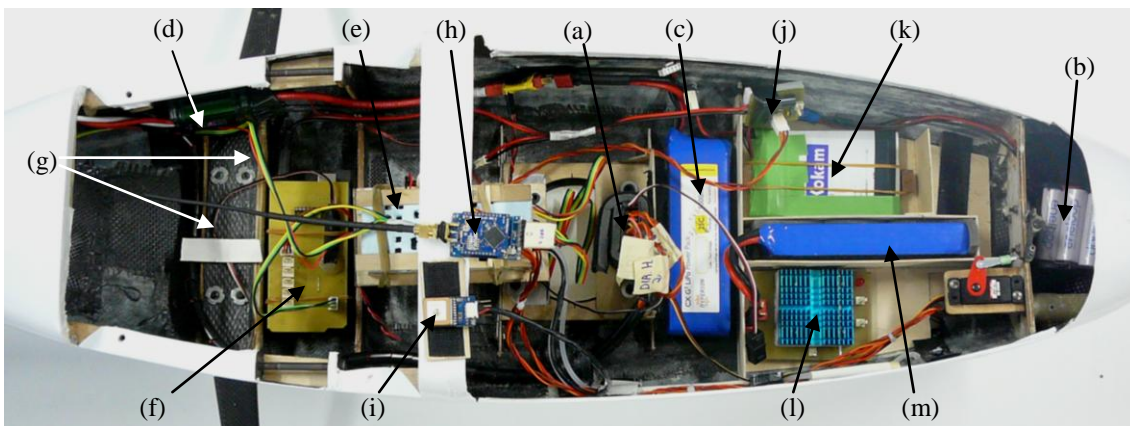


Figure 11: Systems inside the UAV fuselage: (a) 2.4GHz controller receiver and (b) receiver power batteries; (c) electric brushless motor power battery; (d) motor controller; (e) *ArduPilot Mega 1.0*; (f) *Arduino Mega* with sensors electronic shield; (g) RPM and temperature sensors wiring; (h) Xbee telemetry wireless modem and antenna; (i) GPS receiver; (j) *APM1.0* voltage and current sensors; (k) *APM1.0* power battery; (l) VSW servos DC-DC regulator; and (m) VSW servos power battery.

The *ArduPilot Mega* hardware is interfaced and controlled using the *ArduPlane*, an *Arduino* compatible open source autopilot software. This software is very user-friendly and well structured, simplifying the integration of other sub-systems. In fact, several

systems were developed and integrated in *ArduPlane*: for example, an alpha-beta probe with a pitot-static tube. To further expand the capabilities of *APMI.0*, an *Arduino Mega* was connected via the I²C protocol. An electronic shield was developed and adapted to the *Arduino Mega* board to provide connections for motor RPM and temperature, VSW actuator servo's voltage and current, *APMI.0* current and battery voltage and also to interface the load cell (excitation, amplification and acquisition) for measuring in-flight propeller thrust. Figure 11 shows the *ArduPilot Mega* installed inside the fuselage along with all the equipment required to control, power and monitor the UAV platform.

5.2 Flight Performance Tests

Flight performance tests deal with the measurement of the lift-to-drag ratio of the vehicle as a function of airspeed for different VSW positions, from fully extended to fully retracted. For this purpose, the UAV is flown for a given trimmed speed in straight and level flight while the thrust of the propeller is recorded. Since in this condition lift equals weight and drag equals thrust, the lift-to-drag ratio is given by the ratio W/T . This same procedure is repeated for both the VSW and the original fixed wing so that relative gains of the former over the latter are obtained. These results will also be compared with the numerical estimates previously computed.

6 CONCLUSIONS

The main conclusions of the work done in the design and development of a variable-span morphing wing concept are:

- Aerodynamic design optimization showed that the VSW manages to reduce the $drag \times speed$ integral in the design speed range of the vehicle.
- At low speeds, the original wing has slightly better performance than the variable-span wing, due to the performance reduction of the modified SG6042 airfoil, the higher relative thickness ratio of the IFW airfoil and the increased vehicle weight. However, this performance trend is inverted beyond 25.5m/s, in the speed range where retraction of the OMW occurs, which reduces the wing area and consequently the total wing drag. For example, at 35m/s the drag of the VSW was reduced by 22% from the original fixed wing.
- The roll rate with asymmetric wingspan control of the VSW decreases with increasing speed, contrary to what happens for a conventional wing with ailerons. Therefore, the new wing becomes more stable with the increase in speed. Nonetheless, the variable-span wing surpasses, within the operational speed range, the minimum acceptable value for roll rate, from which one can conclude that it can perform steady turns with asymmetric span control, without the need of ailerons.
- Both deployment and load tests revealed satisfactory performance of the VSW concept. However, deployment can be improved in two areas: (a) by increasing the skin stiffness at the IFW tip with an internal stiff rib (between sandwich facings) or with an external lighter rib similar to an end plate around the perimeter of the airfoil; and (b) by decreasing the friction force between the wings with experimentation on the use of ball-bearings and with enhanced surface finishing.
- Flight tests of the VSW are planned for functionality, performance, roll authority and actuation energy evaluation and for collecting data for automatic span control system design. These tests will help quantify the actuation energy requirements during flight to assess whether flight performance improvements justify the increased structural and power related weight and complexity.

REFERENCES

- [1] Tidwell Z, Joshi S, Crossley W, and Ramakrishnan S, Comparison of Morphing Wing Strategies Based Upon Aircraft Performance Impacts, 45th AIAA/ASME/ASCE/AHS/ASC Structures, Structural Dynamics and Materials Conference, Palm Springs, California, 19-22 April, 2004.
- [2] Gamboa P, Vale J, Lau F, and Suleman A, Optimization of a Morphing Wing Based on Coupled Aerodynamic and Structural Constraints, *AIAA Journal*, Volume 47, Number 9, pp. 2087-2104 (2009).
- [3] Neal D, Good M, Johnston C, Robertsha WH, Mason W, and Inman D, Design and Wind-Tunnel Analysis of a Fully Adaptive Aircraft Configuration, 45th AIAA/ASME/ASCE/AHS/ASC Structures, Structural Dynamics and Materials Conference, Palm Springs, California, 19-22 April, 2004.
- [4] Blondeau J, and Pines D, Pneumatic Morphing Aspect Ratio Wing, 45th AIAA/ASME/ASCE/AHS/ASC Structures, Structural Dynamics and Materials Conference, Palm Springs, California, 19-22 April, 2004.
- [5] Cadogan D, Graham W, and Smith T, Inflatable and Rigidizable Wings for Unmanned Aerial Vehicles, 2nd AIAA "Unmanned Unlimited" Systems, San Diego, California, 15-18 September, 2003.
- [6] Scarborough S, Rowe J, Smith S, Simpson A, and Jacob J, Development of a Finite Element Model of Warping Inflatable Wings, 47th AIAA/ASME/ASCE/AHS/ASC Structures, Structural Dynamics, and Materials Conference, Newport, Rhode Island, 1-4 May, 2006.
- [7] Vale J, Leite A, Lau F, and Suleman A, Design and Development of Strategies and Structures for Wing Morphing, The Applied Vehicle Technology Panel Symposium (AVT-168), Évora, Portugal, 20-23 April, 2009.
- [8] Bowman J, Sanders B, and Cannon B, Development of Next Generation Morphing Aircraft Structures, 48th AIAA/ASME/ASCE/AHS/ASC Structures, Structural Dynamics, and Materials Conference, Honolulu, Hawaii, 23-26 April 2007.
- [9] Flanagan JS, Strutzenberg RC, Myers RB, and Rodrian JE, Development and Flight Testing of a Morphing Aircraft, the NextGen MFX-1, 48th AIAA/ASME/ASCE/AHS/ASC Structures, Structural Dynamics, and Materials Conference, Honolulu, Hawaii, 23-26 April 2007.
- [10] Henry J, Blondeau J, and Pines D, Stability Analysis for UAVs with a Variable Aspect Ratio Wing, 46th AIAA/ASME/ASCE/AHS/ASC Structures, Structural Dynamics and Materials Conference, Austin, Texas, 18-21 April, 2005.
- [11] Bae J, Seigler T, Inman D, and Lee I, Aerodynamic and Static Aeroelastic Considerations of a Variable-Span Morphing Wing, 45th AIAA/ASME/ASCE/AHS/ASC Structures, Structural Dynamics and Materials Conference, Palm Springs, California, 19-22 April, 2004.
- [12] Babarino S, Bilgen O, Ajaj RM, Friswell MI, and Inman DJ, A Review of Morphing Aircraft, *Journal of Intelligent Material Systems and Structures*, Volume 22 - June 2011, pp. 823-877 (2011).
- [13] Secanell M, Suleman A, and Gamboa P, Design of a Morphing Airfoil Using Aerodynamic Shape Optimization, *AIAA Journal*, Volume 44, Number 7, pp.

1550-1562 (2006).

- [14] Marques M, Gamboa P, and Andrade E, Design of a Variable Camber Flap for Minimum Drag and Improved Energy Efficiency, 50th AIAA/ASME/ASCE/AHS/ASC Structures, Structural Dynamics, and Materials Conferences, Palm Springs, California, 4-7 May, 2009.
- [15] Mestrinho J, Gamboa P, and Santos P, Design Optimization of a Variable-Span Morphing Wing for a Small UAV, 52th AIAA/ASME/ASCE/AHS/ASC Structures, Structural Dynamics and Materials Conference, Denver, Colorado, 4-7 April, 2011.
- [16] Drela M, XFOIL 6.94 User Guide, Massachusetts Institute of Technology & Astro Harold Youngren Aircraft, Inc., 10 December 2001.
- [17] Gamboa P, Multidisciplinary Design Optimization of Morphing Aircraft, PhD Thesis, Departamento de Ciências Aeroespaciais, Universidade da Beira Interior, Covilhã, December 2007.
- [18] Anderson JD, Corda S, and Wie DM, Numerical Lifting Line Theory Applied to Drooped Leading-Edge Wings Below and Above Stall, *Journal of Aircraft*, Volume 17, Number 12, pp. 898-904 (1980).
- [19] Katz J, and Plotkin A, *Low-Speed Aerodynamics*, McGraw-Hill, 2nd Edition, 1991.
- [20] Mukherjee R, An Iterative Decambering Approach for Post-Stall Prediction of Wing Characteristics Using Known Section Data, 41st AIAA Aerospace Sciences Meeting, Reno, Nevada, 6-9 January, 2003.
- [21] Raymer DP, *Aircraft Design: A Conceptual Approach*, 4th Edition, AIAA Education Series, AIAA, 2006.
- [22] Zhou J, Tits AL, and Lawrence CT, User's Guide for FFSQP Version 3.7, Electrical Engineering Department and Institute for Systems Research, University of Maryland, United States of America, April 1997.
- [23] Secanell M, and Suleman A, Numerical Evaluation of Optimization Algorithms for Low Reynolds Number Aerodynamic Shape Optimization, *AIAA Journal*, Volume 43, Number 10, pp. 2262-2267 (2005).
- [24] Henry J, and Pines D, A mathematical Model for Roll Dynamics by use of a Morphing-Span Wing, 48th AIAA/ASME/ASCE/AHS/ASC Structures, Structural Dynamics, and Materials Conference, Honolulu, Hawaii, 23-26 April, 2007.
- [25] Anon., Flying Qualities of Piloted Airplanes, Military Specification MIL-F-8785C, 5 November 1980.
- [26] Tavares FMT, Roll Motion Control of a Dissymmetrical Wingspan Aircraft, MSc Thesis, Departamento de Ciências Aeroespaciais, Universidade da Beira Interior, Covilhã, October 2011.
- [27] Felício J, Santos P, Gamboa P, and Silvestre M, Evaluation of a Variable-Span Morphing Wing for a Small UAV, 52th AIAA/ASME/ASCE/AHS/ASC Structures, Structural Dynamics and Materials Conference, Denver, Colorado, 4-7 April, 2011.